The 8th European Congress on Computational Methods in Applied Sciences and Engineering
ECCOMAS Congress 2022
5-–9 June 2022, Oslo, Norway

SHAPE OPTIMISATION OF TURBOMACHINERY COMPONENTS

BERNHARD SEMLITSCH AND ALEXANDER HUSCAVA

TU Wien
Getreidemarkt 9/BA, 1060 Vienna, Austria
e-mail: bernhard.semlitsch@tuwien.ac.at, www.tuwien.at

Key words: Computational Fluid Dynamics, Shape Optimisation, Rotating Impeller, Turbomachinery Design

Abstract. Low-order models are the first choice to find the initial design of turbomachinery components screening many configurations. The final optimisation of the three-dimensional geometry is crucial for the best performance. Because of the ability to accurately predict the performance of turbomachinery, fluid dynamic simulations became a powerful tool [10]. However, parameter studies for shape optimisation relying on fluid dynamic simulations are computationally expensive and might fail to reveal the optimal geometry. Gradient-based optimisation approaches allow a significant reduction of simulations and hence, determine the optimum efficiency. The adjoint method finds the optimisation gradient by calculating the derivatives of the state variables with respect to the design objective without the need for finite differences [6]. Thus, the adjoint optimisation is especially efficient for problems with many degrees of freedom and few design objectives, e.g. increasing efficiency. The application of the adjoint method for shape optimisation is demonstrated on the example of a centrifugal compressor impeller. The shape of the rotor blades is optimised, and the impact of different objection functions, i.e. reducing the required moment or increasing the achieved pressure ratio, and optimisation constraints, i.e. retaining the operating point or keeping an area ratio, is analysed. The results demonstrate that the compressor performance can be significantly improved using the adjoint method. However, the challenge is to obtain not only an optimised shape for operating points but also for the entire operating map. The final shapes, obtained for different operating points, are compared.

1 INTRODUCTION

Numerically efficient methods are desired for the initial layout definition of turbomachinery components [2]. Hence, simple thermodynamic formulations are employed, fed with empirical correlations to represent unresolved phenomena, e.g. flow incidence, tip gap losses or trailing edge losses, and allow derivation of the state variables at certain stations. Thereby, many turbomachinery configurations can be screened due to their computational efficiency. This also allows for a holistic system analysis considering the interplay of the components [1, 8].

Two or higher-dimensional models, such as the streamline curvature method [4], are required to shape the initial geometry with parametric design variables, e.g. cord, angle of attack, camber, or tip gap. The computational expense rises because the turbomachinery performance is

evaluated accordingly to the chosen shape parametrisation. Thus, the accuracy is limited by the considered shape parameters and how correct their influence on the turbomachinery performance is modelled. Within this limitation, the turbomachinery geometry can be established and efficiently optimised.

Commonly, the three-dimensional details of turbomachinery geometries are further optimised using three-dimensional flow simulations based on the steady-state Reynolds-Averaged Navier-Stokes (RANS) approach. The modelling assumptions are thereby significantly reduced, but the expense of computational power rises. Sundström et al. [10] employed this approach to predict performance maps for centrifugal compressors and showed its reliability by the satisfactory result comparison with experimental measurement data. Barsi et al. [3] employed an automatic approach for shape optimisation using penalty and objective functions for eight geometrical parameters. Tüchler et al. [11] performed the shape optimisation of a centrifugal compressor with the objective of widening the operating range towards low mass flow rate operating conditions. The RANS approach was combined with a generic algorithm using 13 geometrical parameters.

Parametric optimisation has the disadvantage of many suboptimal configurations being evaluated and later discarded. The local performance gradient, pointing in the optimal shape direction, can be calculated to reduce the number of such computations. The computation via finite differences remains numerically expensive when many shape parameters are considered because flow simulations are required for each shape parameter perturbation. However, the objectives are commonly a few, e.g. efficiency or reduction of losses. The derivative computation of the objective and constraint functions with respect to the state variables can be efficiently performed using the adjoint equations, which are about as costly as two to three flow simulations [5].

We apply the discrete adjoint method for the Navier-Stokes equations to optimise the geometry of a radial compressor impeller. The obtained shapes with different objective functions and optimisers are compared. Further, we describe the challenges arising with shape optimisation when wide operating ranges are desired.

2 METHODOLOGY

The compressible form of the steady-state Reynolds-Averaged Navier-Stokes equations is solved numerically for the determination of the flow state variables and the residuals. The conservation equations are as follows;

$$\nabla \cdot (\varrho \boldsymbol{u}_i) = 0 \ , \tag{1}$$

$$\nabla \cdot (\varrho \boldsymbol{u}_r \boldsymbol{u}_i) = -\nabla p + \mu_{\text{eff}} \nabla \cdot (\nabla \boldsymbol{u}_i + \nabla \boldsymbol{u}_i^T) + \boldsymbol{\omega} \times \boldsymbol{u}_i \ , \text{and} \tag{2}$$

$$\nabla \cdot (\varrho e \boldsymbol{u}_i) + \nabla \cdot \left(\frac{\varrho |u|_i^2}{2} \boldsymbol{u}_i \right) = -\nabla \cdot (p \boldsymbol{u}_i) + \alpha_{\text{eff}} \nabla \cdot (\nabla e) \ , \tag{3}$$

where ϱ is the density, p is the pressure, e is the internal energy, and $\boldsymbol{u}_i$ and $\boldsymbol{u}_r$ are the velocities in the inertial and the relative reference frame. The velocities are related via $\boldsymbol{u}_i = \boldsymbol{u}_r + \boldsymbol{\omega} \times \boldsymbol{x}$, where $\boldsymbol{\omega}$ is the rotational speed vector and $\boldsymbol{x}$ is the coordinate of the cell centre. The effective dynamic viscosity, $\mu_{\text{eff}} = \mu + \mu_t$, and the effective thermal diffusivity, $\alpha_{\text{eff}} = \alpha + \alpha_t$, are composed of the molecular and turbulent components. The Spalart-Allmaras turbulence closure is employed

for modelling of μ_t and α_t due to its capabilities handling flow separation [9],

$$\nabla \cdot (\boldsymbol{u}_i \tilde{\nu}) = \frac{1}{\sigma}\left(\nabla \cdot [(\nu + \tilde{\nu})\nabla\tilde{\nu}] + C_{b2}|\nabla\tilde{\nu}|^2\right) + C_{b1}\tilde{S}\tilde{\nu} - C_{w1} f_w \left(\frac{\tilde{\nu}}{d}\right)^2 , \tag{4}$$

$$\text{with} \quad \mathrm{Pr}_t = \frac{\nu_t}{\alpha_t}, \quad \nu_t = \frac{\mu_t}{\varrho} = \tilde{\nu} f_{v1}, \quad f_{v1} = \frac{\chi^3}{\chi^3 + C_{v1}^3}, \quad \chi = \frac{\tilde{\nu}}{\nu} ,$$

$$\tilde{S} = S + \frac{\tilde{\nu}}{\kappa^2 d^2} f_{v2}, \quad f_{v2} = 1 - \frac{\chi}{1 + \chi f_{v1}}, \quad S = \sqrt{2\Omega_{ij}\Omega_{ij}}, \quad \Omega_{ij} = \frac{1}{2}\left(\nabla \boldsymbol{u}_i - (\nabla \boldsymbol{u}_i)^T\right) ,$$

$$f_w = g\left[\frac{1 + C_{w3}^6}{g^6 + C_{w3}^6}\right]^{1/6}, \quad g = r + C_{w2}(r^6 - r), \text{ and } \quad r = \frac{\tilde{\nu}}{\tilde{S}\kappa^2 d^2} ,$$

where $\tilde{\nu}$ is the Spalart-Allmaras variable, d is the distance to the closest surface, and κ, σ, C_{b1}, C_{b2}, C_{v1}, C_{w1}, C_{w2}, C_{w3}, and Pr_t are constants with the standard values provided by Spalart and Allmaras [9]. The principle idea behind the Spalart-Allmaras turbulence closure is to impose a quartic behaviour of the variable $\tilde{\nu}$ close to walls, which mimics the inherent profile relation between ν_t and y^+ [7]. This allows the use of less accumulated cells at the wall to predict the correct distribution of ν_t. This feature is very valuable facilitating the mesh movement in between optimisation cycles without quality degeneration.

The governing flow equations are solved using the SIMPLEC algorithm. The gradients are discretised with a cell-limited least-squares scheme. For the divergence and laplacian terms, a second-order upwind scheme and a second-order central scheme are employed.

2.1 Adjoint equations

The discrete adjoint method is employed to optimise the blade shape of the centrifugal compressor impeller. The advantages of the discrete over the continuous adjoint method are the lower dependence of mesh resolution, consistency with the flow solvers, robustness, and the practicability to realise complex objective functions. The discrete adjoint formulation is based on the discretised governing equations to compute the total derivative of the objective or constraint function, f, with respect to the design variables, $\boldsymbol{x}$, or control points representing the design space. The objective or constraint function, f, is a function of both; the design variables, $\boldsymbol{x}$, and the state variables, $\boldsymbol{w}$. Thus, the total derivative can be expressed via the chain rule as,

$$\frac{df}{d\boldsymbol{x}} = \frac{\partial f}{\partial \boldsymbol{x}} + \frac{\partial f}{\partial \boldsymbol{w}}\frac{d\boldsymbol{w}}{d\boldsymbol{x}} . \tag{5}$$

The partial derivatives $\partial f/\partial \boldsymbol{x}$ and $\partial f/\partial \boldsymbol{w}$ can be computed explicitly. The computation of the total derivative matrix, $d\boldsymbol{w}/d\boldsymbol{x}$, is expensive because of the implicit relation via the discrete residual equations, $\boldsymbol{R}(\boldsymbol{w}, \boldsymbol{x}) = 0$. The discrete residual equations are obtained from the flow solver and applying the chain rule to the discrete residual equations leads to,

$$\frac{d\boldsymbol{R}}{d\boldsymbol{x}} = \frac{\partial \boldsymbol{R}}{\partial \boldsymbol{x}} + \frac{\partial \boldsymbol{R}}{\partial \boldsymbol{w}}\frac{d\boldsymbol{w}}{d\boldsymbol{x}} = 0 \rightarrow \frac{d\boldsymbol{w}}{d\boldsymbol{x}} = -\frac{\partial \boldsymbol{R}^{-1}}{\partial \boldsymbol{w}}\frac{\partial \boldsymbol{R}}{\partial \boldsymbol{x}} . \tag{6}$$

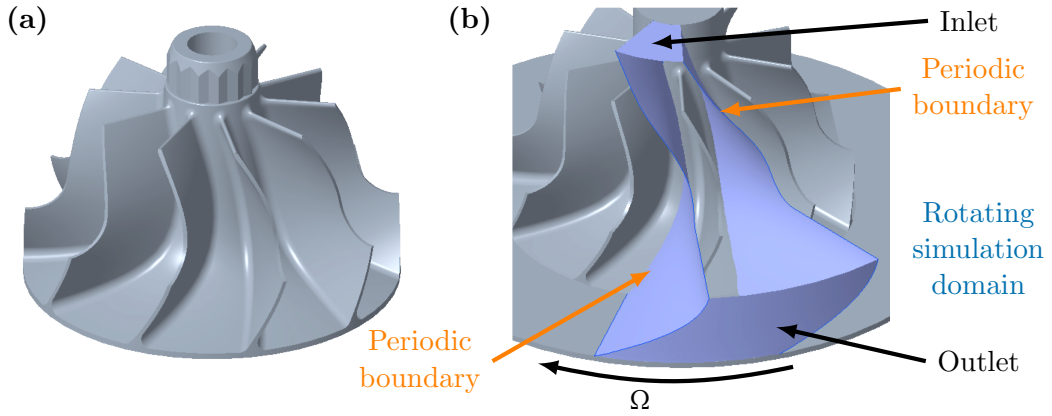

Figure 1: The centrifugal compressor geometry is shown beside of the computational domain with the applied boundary conditions.

This expression can now be substituted into eq. 5, which gives

$$\frac{df}{d\boldsymbol{x}} = \frac{\partial f}{\partial \boldsymbol{x}} - \underbrace{\frac{\partial f}{\partial \boldsymbol{w}} \frac{\partial \boldsymbol{R}^{-1}}{\partial \boldsymbol{w}}}_{\boldsymbol{\psi}^T} \frac{\partial \boldsymbol{R}}{\partial \boldsymbol{x}} \ . \tag{7}$$

The adjoint vector, $\boldsymbol{\psi}$, can be calculated solving the equation,

$$\frac{\partial \boldsymbol{R}^T}{\partial \boldsymbol{w}} \boldsymbol{\psi} = \frac{\partial f^T}{\partial \boldsymbol{w}} \ . \tag{8}$$

The transpose of the adjoint vector, $\boldsymbol{\psi}$, is finally used to solve the total derivative given in eq. 5. Noteworthy is that the design variable is not explicitly present in eq. 8. Thus, the computational cost of the evaluation is independent of the number of design variables but related to the number of objective or constraint functions. With a few target functions and many design variables, such circumstances are typical for engineering design applications.

2.2 Case Setup

The optimisation methodology is applied to the geometry of a centrifugal compressor with 10 full impeller blades, which is shown in figure 1. Only one blade passage is considered for the optimisation, and periodic boundary conditions are set. The tip gap is 1 mm. The rotational speed of the impeller is set to a constant value accordingly to the operating point. The boundary conditions at the inflow are set to atmospheric conditions, i.e. $p_{t,\mathrm{in}} = 101325$ Pa and $T_{t,\mathrm{in}} = 293.15$ K. Zero gradient boundary conditions are specified at the outlet for pressure and temperature. The mass flow rate is specified at the outlet, and zero gradient boundary conditions are set for the velocity at the inlet. No-slip boundary conditions are set with wall functions for ν_t towards all walls. The inlet value is set correspondingly to the turbulent length scale, l, and a turbulent intensity of $I = 5$ %, where $\tilde{\nu} = \nu_t = C_\mu k^2/\varepsilon$, $k = 3\ \overline{u}_{\mathrm{in}}^2 I^2/2$, and $\varepsilon = C_\mu k^{3/2}/l$ ($\overline{u}_{\mathrm{in}}$ is the average velocity at the inlet and C_μ is a constant). A zero gradient boundary condition is set for ν_t at the outlet.

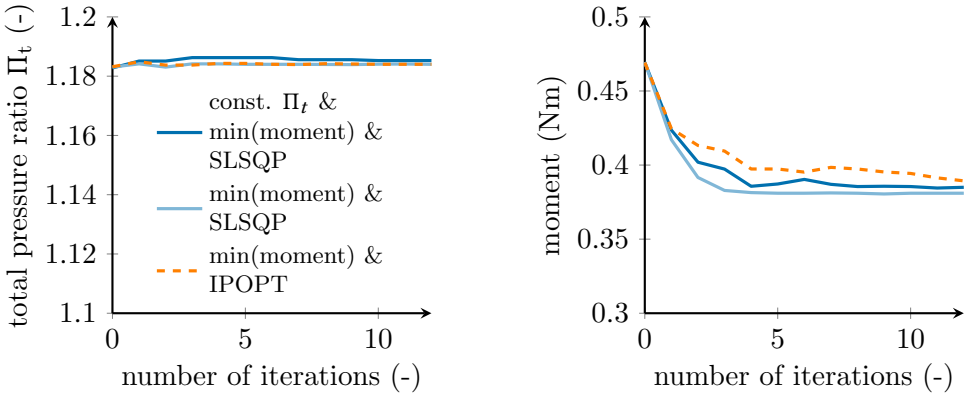

Figure 2: Comparison of the obtained global performance parameters for different objective functions and optimisers.

2.3 Numerical Mesh

A single blade passage is considered due to the rotational periodicity. An unstructured mesh is preferred for the purpose of optimisation because the mesh quality deteriorates quickly during the optimisation, and the geometry can be automatically re-meshed at any time needed. The mesh has been refined towards all walls, the tip gap region, and the leading and trailing edges.

3 RESULTS

The aims of the present investigation are twofold: analysing the impact of different objective functions and constraints and comparing the shape optimisation results obtained for different operating conditions.

3.1 Objective Functions and Constraints

The objective function of the optimisation represents the design target. Under certain geometrical or physical constraints, this objective function value will be maximised or minimised with the optimiser. The efficiency, the achieved total pressure ratio, or the required moment are common aims in the case of a centrifugal compressor. We aim to reduce the required moment for the presented example to achieve the same total pressure ratio. Further, it is assumed that low-order models have optimised the inflow and outflow cross-sections. Thus, only the three-dimensional blade shape is considered for optimisation. The constraints are set accordingly, where the blade thickness and the tip gap are fixed over the shape optimisation. A rotational speed of $50,000$ rpm at an intermediate mass-flow rate is specified as the operating condition.

First, the results for two optimisers, i.e. the Sequential Least SQuares Programming (SLSQP) optimiser and the Interior Point OPTimizer (IPOPT), are compared, where the achieved global performance values are plotted in figure 2. The reduction of the required moment was solely specified as the objective function. The total pressure ratio remained nearly constant with both optimisers, but significant differences can be observed in the required moment. The SLSQP optimiser leads to better performance and convergence rate. Therefore, the SLSQP optimiser is employed for the remainder of the work.

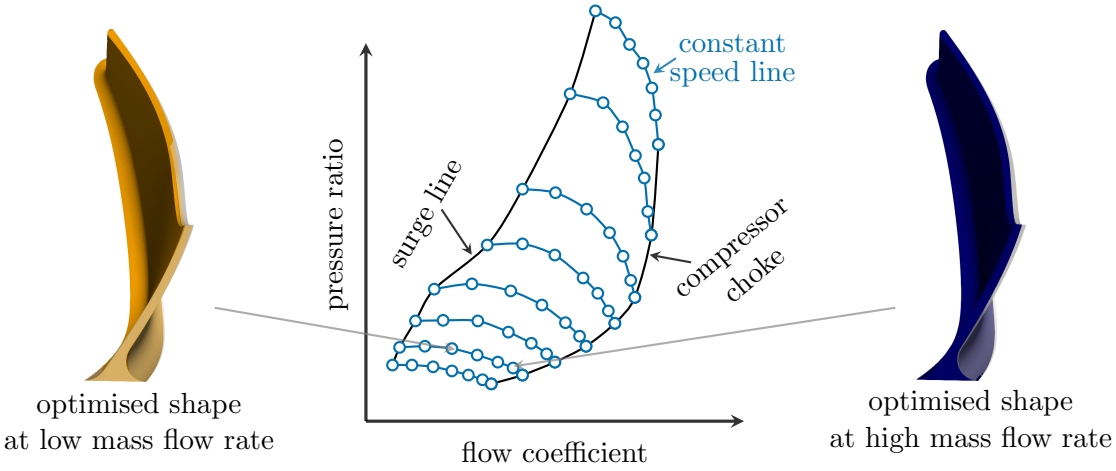

Figure 3: The different geometrical impeller blade shapes obtained at different operating conditions are illustrated, where the rotational speed is 50,000 rpm. The initial geometry shape is shown transparently.

Figure 2 exhibits that the total pressure ratio, $\Pi_t = p_{t,out}/p_{t,in}$, increases slightly when additionally a constrain is set for the total pressure ratio. Without the specific constrain to keep the total pressure ratio constant, the total pressure ratio rises initially less, and a lower required moment can be achieved. It is, however, expected that the optimised shape converges to the same solution, but more optimisation iterations are required.

3.2 Operating Conditions

Centrifugal compressors are utilised in many applications. For some applications, e.g. turbochargers, the width of the operating range is of higher importance than the peak efficiency at the nominal design point because the centrifugal compressor is mainly employed at off-design operating conditions. Thus, the adjoint method is used to optimise the compressor impeller blade under various operating conditions, where the SLSQP optimiser is used with the sole objective function of reducing the required moment. Converged steady-state flow solutions are needed for optimisation. Thus, only operating conditions for which steady-state flow solutions can be obtained are considered.

Figure 3 shows that the optimised blade shapes for low and high-mass flow-rate operating conditions can be dissimilar. Differences can be mainly observed at the trailing edge and the blade curvature. The obtained shapes illustrate the shape complexity that can be obtained, which is challenging to be described via parameters. The optimisation alterations remain small because of the initial design quality. The final shape needs to be averaged (considering the sensitivities) with a weighting favouring the operating conditions that will occur most likely to achieve the best impeller blade shape from the individual optimisations. The impeller blade shape at the lowest mass flow rate will have the highest weight to widen the operating range of the centrifugal compressor.

4 CONCLUSIONS

The discrete adjoint method has been successfully applied to optimise the blade shape of a centrifugal compressor impeller. The optimisation results using different optimisers, objective functions, and constraints have been presented. It was shown that the discrete adjoint method allows complex geometrical optimisation without tedious geometry parametrisation. The best results have been obtained using the Sequential Least SQuares Programming (SLSQP) optimiser with the objective to reduce the moment and the least amount of constraints.

The application of the discrete adjoint method for shape optimisation to increase the turbomachinery efficiency at the nominal operating condition is straightforward. Shape optimisation to widen the operating range is challenging because several operating conditions need to be regarded. The optimisation has been performed for several operating conditions, which lead to different geometries. The shapes and the sensitivities obtained for different operating conditions need to be averaged with a certain weighting function. Such weighting functions should favour the optimisation results at low mass flow rate conditions to widen the operating range. However, this introduces a penalty at high-performance and high mass flow rate operating conditions. Thus, a reasonable balance needs to be found for the weight distribution, which depends on the particular aims of the manufacturer.

Presently, the optimisation is limited by the memory requirements of the computation. Therefore, the numerical domain was reduced to a single blade passage. This setup restricts the optimal shape solutions. For example, the improvement at low mass flow rate conditions due to varying (circumferentially non-uniform) blade pitch angles cannot be captured. Hence, the minimisation of the memory requirements is targeted in the future.

REFERENCES

[1] Asgari, H., Venturini, M., Chen, X., and Sainudiin, R. Modeling and simulation of the transient behavior of an industrial power plant gas turbine. *Journal of Engineering for Gas Turbines and Power 136*, 6 (2014).

[2] Aungier, R. H. Turbine aerodynamics. *American Society of Mechanical Engineers Press, New York* (2006).

[3] Barsi, D., Costa, C., Cravero, C., and Ricci, G. Aerodynamic design of a centrifugal compressor stage using an automatic optimization strategy. In *Turbo Expo: Power for Land, Sea, and Air* (2014), vol. 45615, American Society of Mechanical Engineers, p. V02BT45A017.

[4] Casey, M., and Robinson, C. A new streamline curvature throughflow method for radial turbomachinery. *Journal of Turbomachinery 132*, 3 (July 2010), 031021–10.

[5] He, P., Mader, C. A., Martins, J. R., and Maki, K. J. Dafoam: An open-source adjoint framework for multidisciplinary design optimization with openfoam. *AIAA journal 58*, 3 (2020), 1304–1319.

[6] Jameson, A. Aerodynamic design via control theory. *Journal of scientific computing 3*, 3 (1988), 233–260.

[7] Kalitzin, G., Medic, G., Iaccarino, G., and Durbin, P. Near-wall behavior of rans turbulence models and implications for wall functions. *Journal of Computational Physics 204*, 1 (2005), 265–291.

[8] Nikolaidis, T., Wang, H., and Laskaridis, P. Transient modelling and simulation of gas turbine secondary air system. *Applied Thermal Engineering 170* (2020), 115038.

[9] Spalart, P., and Allmaras, S. A One-Equation Turbulence Model for Aerodynamic Flows. Tech. rep., American Institute of Aeronautics and Astronautics, 1992. AIAA-92-0439.

[10] Sundström, E., Semlitsch, B., and Mihăescu, M. Similarities and differences concerning flow characteristics in centrifugal compressors of different size. In *Proceedings of the 5th International Conference on Jets, Wakes and Separated Flows (ICJWSF2015)* (2016), Springer, pp. 457–464.

[11] Tüchler, S., Chen, Z., and Copeland, C. D. Multipoint shape optimisation of an automotive radial compressor using a coupled computational fluid dynamics and genetic algorithm approach. *Energy 165* (2018), 543–561.